THE ASTROPHYSICAL JOURNAL, 418:123–134, 1993 November 20

TRACING THE STELLAR MASS IN M51

HANS-WALTER RIX[1]
Institute for Advanced Study, Princeton, NJ 08540
AND
MARCIA J. RIEKE
Steward Observatory, University of Arizona, Tucson, AZ 85721
Received 1993 March 5; accepted 1993 June 1

ABSTRACT

We present optical and IR surface photometry of M51 (NGC 5194) at *B*, *V*, *R*, *I*, *J*, *K*, and CO(2.3 μm). These data are used to establish whether *K* band (2.2 μm) images of spiral galaxies provide reliable maps of stellar surface mass density features such as massive spiral arms or bars. The main distorting agents in the mapping at shorter wavelengths are dust extinction and luminous young stars. From modeling the color changes across the main dust lanes in M51, we find the optical depths to be ~ 0.5 in the *K* band. For these optical depths the *K* band flux is attenuated by only $\lesssim 10\%$ even in the dust lanes. From monitoring the gravity-sensitive CO(2.3 μm) index across the spiral arms we find that young, red supergiants do not distort significantly the *K* band image except in one small patch. OB associations are visible in the *K* band images but only cover a very small fraction of the spiral arms. On this basis, *we conclude that K band images of face-on galaxies do trace the massive disk star population and allow a mapping of the azimuthal variation in the surface mass density of the stellar disk.* In M51 we find the surface mass density contrast (arm/interarm) to range from 1.8 to 3, comparable to results from *N*-body simulations of the galaxy's tidal encounter with NGC 5195. This density contrast is *larger* than the light contrast in *I* band images, where the spiral arm crest is affected by dust extinction. The spiral arm amplitudes in M51 clearly show smooth, strong radial variations, with a maximum at $\sim 130''$ and minima at $45''$ and $170''$. These variations may arise from interference of a pre-existing spiral pattern with the tidally induced spiral arms. An ongoing *K* band imaging study of a sample of spiral galaxies will yield a more representative picture of the role of bars and massive spiral arm features.

Subject headings: dust, extinction — galaxies: individual (M51) — galaxies: ISM — galaxies: photometry — galaxies: spiral — galaxies: structure

1. INTRODUCTION

The surface brightness in elliptical galaxies appears to map the stellar surface mass density very well (except for very shallow radial gradients in the M/L). In contrast, it is difficult to map variations in the stellar surface mass density in spiral galaxies. The mapping is complicated both by the prominent dust lanes and patches in many spirals and by young stars which may contribute much to the light in many colors but only little to the total stellar mass (e.g., Schweizer 1976). Mapping the azimuthal surface mass density variations in spiral galaxies is important in several respects: first, it allows one to make an unbiased estimate of the frequency of bars in spiral galaxies. Some bars only become apparent in the infrared. Second, mapping the position and amplitude of massive spiral arms is important both for testing density wave theory and for comparing dynamical simulations of tidally induced spiral arms (e.g., Toomre & Toomre 1972; Hernquist 1990) directly to observations. Furthermore, this mapping allows us to check whether galaxies with flocculent or chaotic spiral arms (in young stars) have any organized underlying density fluctuation. Finally, we can see how the spiral arm mass amplitude in isolated spiral galaxies correlates with the current star-formation rate, as expected if the spiral structure is driven by star formation.

In this paper we employ optical and IR surface photometry of M51 to establish firmly that *K* band imaging with IR arrays is a reliable and efficient way to map surface *mass* variations[2] through surface *brightness* variations in face-on galaxies. To this end we will show that neither dust nor young, luminous, red stars strongly affect the *K* band image, so that it indeed traces mostly the massive disk star population.

We use M51 for this initial effort because it is a nearby galaxy, yet not too large to be imaged, and because it is the prototype of a grand design spiral. Furthermore, previous observations have shown tentative evidence of a central bar which our data can confirm. It is important to keep in mind that, due to the recent encounter with NGC 5195, M51 is in an atypical dynamical state, and hence conclusions about the properties of its spiral arms must not be generalized.

Aside from these scientific questions we also will address some more technical aspects of infrared surface photometry. No body of near-infrared surface photometry which could be used to define the typical run of colors and surface brightnesses currently exist. Most studies to date have concentrated on starburst or Seyfert galaxies with the exception of the study by Peletier & Willner (1991) of Virgo spirals and of the study by Wainscoat, Hyland, & Freeman (1990) of edge-on galaxies where the surface brightnesses are much higher than in face-on objects. Therefore it appears worthwhile to examine the accuracy, and limitations, of such data sets.

[1] Hubble Fellow.

[2] The light in the *K* band is of course dominated by giants, which make up only a small fraction of the stellar mass. However, for an old population giant stars have the same spatial distribution as the main-sequence stars.

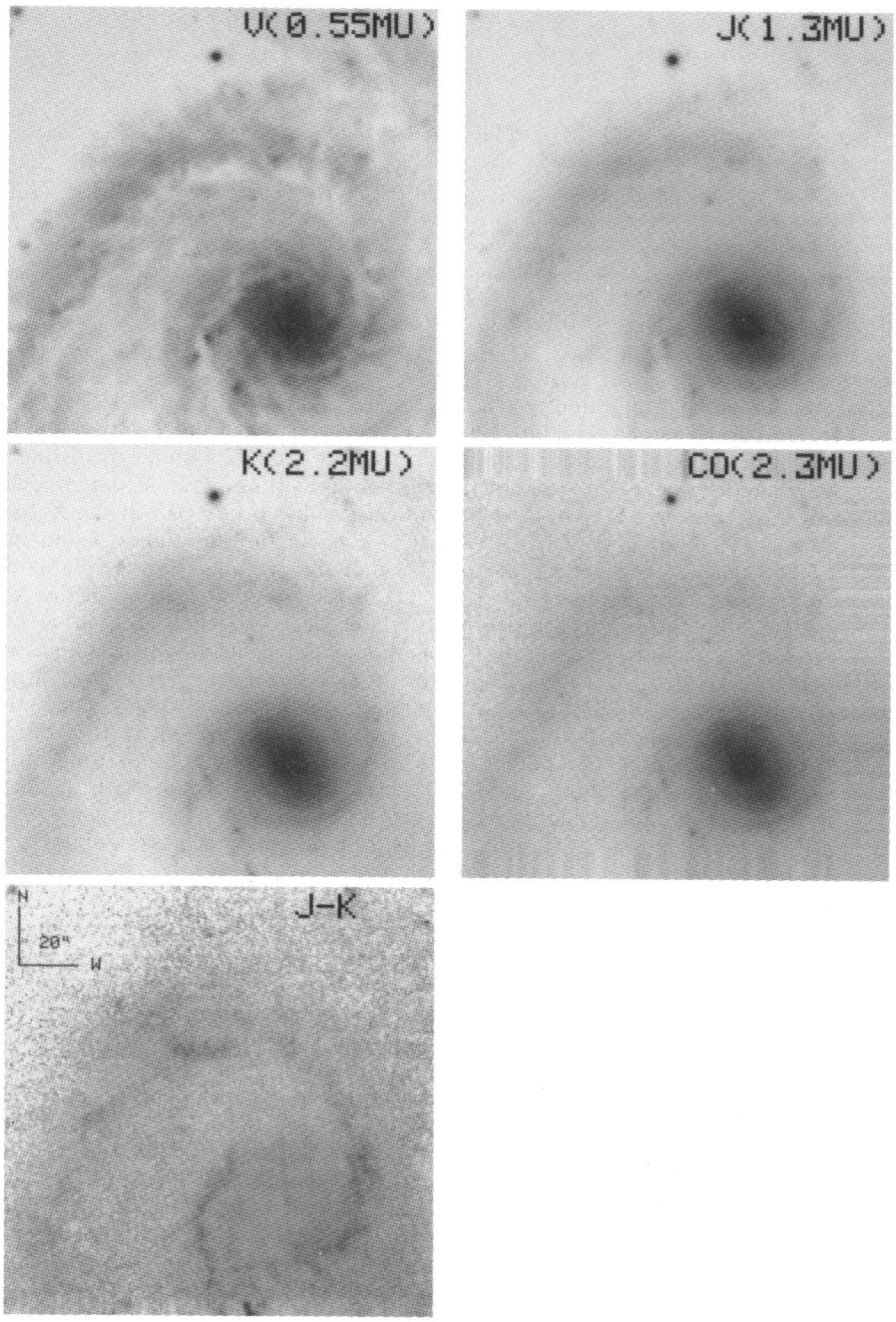

FIG. 1.—7.2 × 7.3 images of M51 in *B*, *V*, *R*, *I*, and *K*. The *K* band image is a mosaic of five images. West is up and north is to the right. The pixel scale is 1.″8 pixel^{-1} as indicated by the 60″ bars in the *B* band image. The optical images have been binned to the same resolution as the *K* band image. Note that in all bands shortward of 1 μm the major dust lanes associated with the spiral arms are still prominent. The impact of dust only becomes small at *K*.

The remainder of the paper is organized as follows: in § 2 we describe the observations and data reduction procedures; in § 3 we analyze and model the data to address the questions raised above; and in § 4 we summarize and discuss the results.

2. OBSERVATIONS AND DATA REDUCTION

The data collected for the present work are comprised of "optical" CCD data (in *B*, *V*, *R*, *I*, and Hα) and IR data (*J*, *K*, and CO 2.3 μm) acquired with NICMOS2 and NICMOS3 arrays. Since the data reduction procedures are quite different for the two sets, we will describe them separately in the following paragraphs.

2.1. *CCD Data*

The data were obtained on 1989 September 4 at the Steward 2.3 m telescope on Kitt Peak with a focal reducer, using a TI CCD, with 800 × 800 pixels of 0.″55 each and a field of view of 7.′3 × 7.′3. The exposure times for the images were 90 seconds for *V*, *R*, and *I*, 120 seconds for *B*, and 300 seconds for Hα. Flat-fielding was done with dome and twilight flats and is good

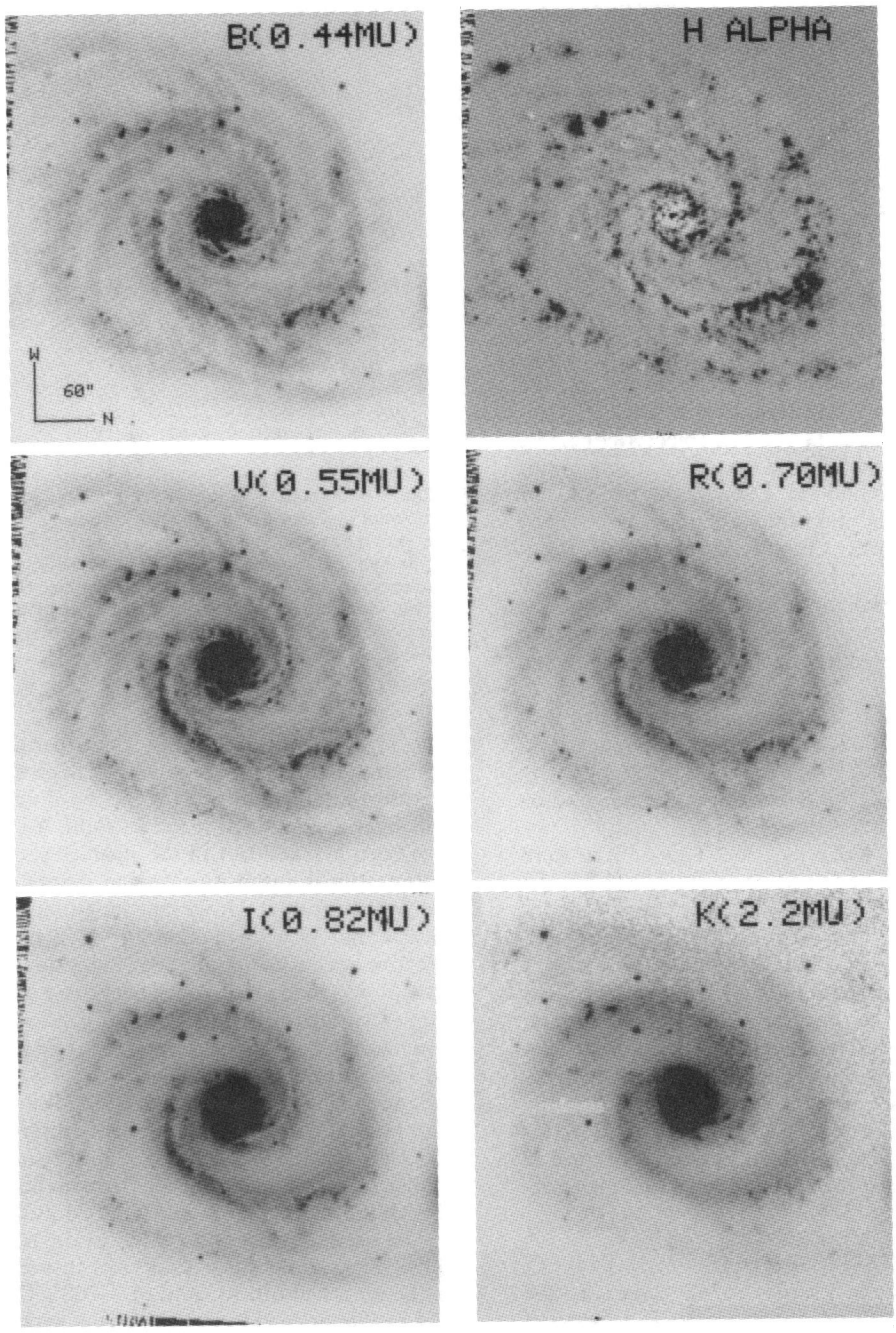

FIG. 2.—2.5 × 2.5 images of M51 in V, J, K, CO(2.3 μm) and $J-K$. Images of the central region of M51 in V, J, K, and CO(2.3 μm) taken with the NICMOS3 camera at 0.″6 pixel^{-1}. Orientation and scale of the image are indicated in V band image. The K band image shows very clearly the central bar. The $J-K$ color image outlines the position of the strongest dust lanes.

to ~1% over the inner 5′ × 5′. The images were calibrated using CCD standard fields in M67 (Schild 1983). The uncertainty in the zero points of the photometry in the various bands is estimated to be 0.05 mag from internal comparisons and from comparison with Schweizer (1976) and Boroson, Strom, & Strom (1981). However, the shape of the luminosity and color profiles presented below depend only on the linearity of the array and the sky subtraction and are therefore constrained better than the zero point at small radii ($4'' \lesssim R \lesssim 100''$). For an uncertainty in the sky level of about 0.5% (variance of sky level in four "empty" patches) the error in the luminosity profiles exceeds 10% outside of 150″.

As a last step in the reduction the CCD images were rotated and rebinned to the K band image of lower spatial resolution (see below). Images in all bands are shown in Figures 1 and 2.

2.2. *IR Data*

The data for the K band mosaic of M51, shown in Figure 1*f*, were obtained on 1989 April 15 at the Steward 1.5 m telescope on Mount Bigelow. The detector was a 128 × 128 NICMOS2 array, with a scale of 1.″8 pixel^{-1}. One frame of the mosaic was centered on the nucleus of M51, while the other four frames had the nucleus about 20 pixels from each corner of the array; the final mosaic encompassed an area of about 7.′2 × 7.′3.

At 2.2 μm the sky is the dominant signal at virtually all points of the image. Therefore, careful monitoring of the sky is mandatory. To this end the telescope was wobbled after each 60 second exposure on the target to a patch of sky offset by about 10′ where an equally long sky exposure was taken. The total integration time (on the object) was about 20 minutes per mosaic patch. The object-sky data stack was reduced as follows (see also Rix 1991 for more details): each frame was bias-subtracted and all bad pixels (covering less than 0.5% of the total area) were replaced by the median value of the surrounding eight pixels. Then, each object frame was flat-fielded by dividing it by the normalized average of the two bracketing sky frames. Finally, a first guess of the sky background was removed by subtracting the mode of the counts levels over the flat-fielded image. These procedures result in a stack of typically 10 to 20 sky-subtracted and flat-fielded object frames. The images in this stack are then aligned spatially, using point sources in the frames, and co-added. Finally, the five mosaic pieces were aligned and combined into a single image using software kindly provided by R. Guhathakurta and G. Bernstein. To make a first-order correction for any tilts in the final image, arising from the mosaicking, we fitted a plane to the same patches of sky which had no detectable galaxy signal in the CCD frames and subtracted it. The final picture is shown in Figure 1*f*.

The flux calibration of the image was achieved by integrating the sky-subtracted flux in the image in concentric annuli and comparing the result to the aperture photometry by Aaronson (1977). We estimate the K zero point to be good to 0.05 mag (Fig. 3).

Further data at J(1.3 μm), K(2.2 μm), and CO(2.3 μm) were obtained at the Steward 2.3 m telescope using a NICMOS3 array on 1992 January 23. These data have much higher resolution: 0.″6 pixel^{-1} (with 1.″2 seeing), but only cover an area of 2.′4 × 2.′4. These data were reduced and calibrated as described above, and the K band data provide an excellent external accuracy check, since they were taken at a different spatial resolution, with a different detector on a different telescope. These images are shown in Figures 2*a*–2*c*. Again, aperture photometry from Aaronson (1977) was used to flux calibrate the J and K frames. The CO(2.3 μm) filter used in this present work deviates from the standard passband (Frogel et al. 1978) and we will only use it for differential spatial measurements.

2.3. *Photometric Profiles and Colors*

We present the photometric profiles in all colors as the surface brightness averaged in concentric annuli as a function of the mean radius of the annulus, rather than fitting ellipses to the image. This is done because M51 is seen nearly face-on and because the ellipse fitting would be dominated by the spiral arms over a significant range in radii. All strong point sources have been masked out in the profiles shown here. The global light profile is insensitive to the details of the point source removal, even in B. However, the global colors do include the spiral arms. As we will show in § 3 in more detail there is no objective way to separate arm from interarm regions and no attempt was made to do so. There can be a large variation ($\gtrsim$1 mag) in surface brightness at any given radius and a 0.3 mag dispersion in color at each surface brightness, arising, e.g., from OB associations and dust lanes.

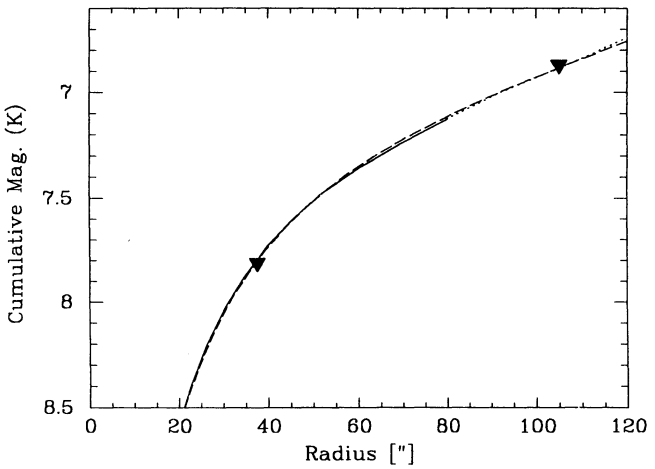

FIG. 3.—Calibration of the IR photometry. We compare the cumulative magnitudes in J and K (as measured from the surface photometry presented here) with the aperture measurements by Aaronson (1975), shown as triangles. The dashed line represents the data from the 7′ × 7′ mosaic; the solid line represents the high-resolution data. The solid line is continued as a dotted line for radii where the data do not provide full azimuthal coverage (see Fig. 2). For the two apertures the agreement is excellent (0.03 mag), and we use Aaronson's measurements for the absolute flux calibration.

Figure 4 shows the profiles in all colors and Table 1 lists all colors and their gradients separately for the bulge and disk. The J band data and some of the K band data extend over a smaller radial range because of the smaller area covered by the NICMOS3 data. The K band data in the overlapping region may be used to judge the quality of the K band surface photometry. These data show that even in the infrared useful data can be obtained out to radii of ~200″. The "shoulder" in the light profile at ~15″ arises from the small central bar in M51

TABLE 1

SUMMARY OF THE GLOBAL COLORS AND COLOR GRADIENTS

	Bulge 3″–15″				Disk 20″–180″			
Bands	C	Δ	$dC/d\ln R$	Δ	C	Δ	$dC/d\ln R$	Δ
$I-K$	1.98	0.04	−0.03	0.08	1.88	0.12	−0.34	0.10
$I-J$	0.95	0.03	0.04	0.04	...	...	...	...
$I-R$	−0.55	0.03	0.02	0.02	−0.53	0.04	0.04	0.04
$I-V$	−1.14	0.04	0.22	0.05	−1.02	0.04	0.32	0.08
$I-B$	−1.97	0.04	0.36	0.07	−1.75	0.07	0.58	0.10

NOTES.—All colors are with respect to I. The colors and their gradients are listed separately (in magnitudes) for the bulge, 3″ < R < 15″, and the disk, 20″ < R < 180″. The estimated uncertainties to not include possible offsets in the optical to IR color normalization.

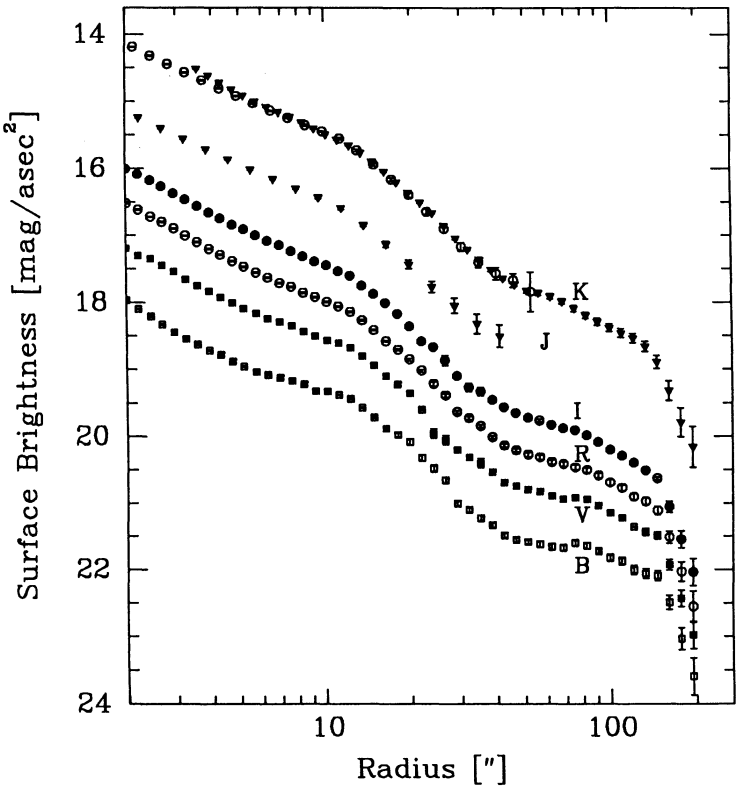

FIG. 4.—Radial luminosity profiles of M51 in *B*, *V*, *R*, *I*, *J*, and K.This figure shows the radial profiles in all bands measured. The flux in each band was sampled in concentric annuli, after removing point sources. The error bars shown include both statistical errors and the uncertainty in the sky level. Only the central part of M51 was imaged in *J*, hence these data have a smaller radial extent. The *K* band profile from the mosaic with the NICMOS2 camera and the high-resolution data with the NICMOS3 camera are overplotted as the top profile.

which becomes very clear in the infrared; its properties will be discussed elsewhere (Zaritsky, Rix, & Rieke 1993).

Figure 5 shows the radial run of the optical and IR colors. The flatness of the $R-I$ profile [$\Delta(I-R) \lesssim 0.04$ mag], which should be insensitive to population changes and dust (see § 4.1.2), can be used to check the reliability of the optical color profiles.

3. ANALYSIS

3.1. *Global Colors and Color Gradients*

3.1.1. *Comparison with Previous IR Aperture Photometry*

Except for a few cases of edge-on galaxies (Wainscoat et al. 1990) and Virgo spirals (Peletier & Willner 1992) the available photometric information in the IR on disk galaxies stems from aperture photometry (Aaronson 1977; Bothun et al. 1985). The good agreement between the integrated surface photometry and aperture photometry (§ 2.2), along with the smoothness of the $J-K$ color profile (Fig. 5) and the IR surface photometry of ellipticals (Peletier 1989 and Rix 1991), reaffirms the quantitative reliability of IR surface photometry with detector arrays. The globally averaged $J-K$ color, 0.95 mag, and an estimate of $B-H$,[3] 3.5 mag, agree well with values found by Bothun et al. (1985) for more distant spiral galaxies with an absolute magnitude in *B* of ~ -20.5.

[3] This estimate assumes that $H = J + 0.3(K-J)$.

3.1.2. *Dust and Global Color Changes*

It is tempting to use this data set to test claims made in a flurry of recent papers (e.g., Disney, Davies, & Phillips 1989; Valentijn 1990) that the disks of spiral galaxies are opaque at optical wavelengths due to dust extinction. If this were the case then the optical and IR colors should be affected by such dust. Disney et al. (1989 have stressed that the color changes for a given optical depth may be smaller than expected for the usual "source–dust screen–observer" geometry, because the dust is mixed in with the stars. Considerable amounts of dust may therefore cause only small color changes.

Virtually all previous authors have only accounted for *absorption* when quantifying the optical depths which are consistent with the observed colors. Dust *scattering* has always been neglected, with the notable exception[4] of D. Elmegreen (1980). Since the (isotropic) albedo of typical dust grains (see, e.g., Draine & Lee 1984) in the optical is about 0.4, almost as many photons are reflected as are absorbed. Thus a dust layer in the disk plane does not only act as a sink for the light behind it, but also as a mirror. Using the simplified radiative transfer model described in the Appendix, we can illustrate how the colors of M51 [assumed to be seen at cos (*i*) = 0.9] change with increasing optical depth, assuming the dust has a scale height

[4] Witt, Thronson, & Capuano (1992) and Bruzual, Magris, & Calvet (1988) included scattering into their calculations but did not discuss the applicable geometry of plane parallel stratifications of dust and stars with different vertical scale heights.

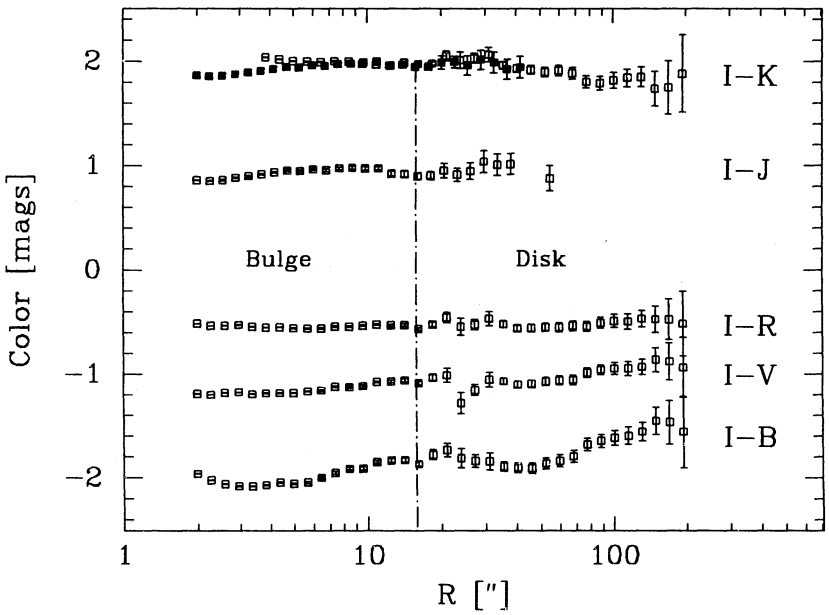

FIG. 5.—Radial color profiles of M51 with respect to *I*. This figure shows the radial color profiles with respect to *I* for all measured bands. The dash-dotted line indicates the approximate radius of the transition from the bulge to the disk. The optical data are only shown to radii to which reliable *K* band surface photometry was obtained.

equal to 0.4 times that of the stars. The relative scale height was chosen to be comparable to those found for the dust lanes in M51 (see § 3.2). Figure 6 shows the change relative to the dust-free case for all the colors shown in Figure 5 and listed in Table 1. Note that for small optical depths and face-on orientations the optical fluxes are slightly enhanced compared to *K*, where scattering is less important. This is because in plane-parallel geometry the change of scattering a photon which is moving in the disk into the normal direction is greater than the chance of scattering a photon which is already moving perpendicularly out of the disk. Hence, scattering effectively redirects a fraction of the photons moving in the disk plane into the face-on direction.

Only for optical depths larger than $\tau_V = 1$ do the color changes from dust reddening become larger than the observed gradients within M51. If we assume that any smoothly distributed dust has a radial scale length comparable (say, within a factor of 2) to the stars' and if we assume that the outer parts of the disk are transparent at *K*(2.2 μm), we can derive limits on the amount of global dust extinction by assuming that *all* the observed inward reddening in M51 is due to dust. Using the color gradients from Table 1 and comparing it to Figure 6 shows that the observed overall color changes could be produced by $\tau_V \sim 1$. Thus much larger optical depths, $\tau_V \gg 1$ can be ruled out on the basis of this data set (in conflict with Valentijn's claim), but no tight limits on τ_V can be derived. In turn, Figure 6 illustrates that for face-on disks the observed global colors are insensitive to the dust content ($\Delta \lesssim 0.05$) for optical depths of $\tau \lesssim 0.5$.

3.1.3. *Optical-IR Color Gradient*

It is apparent from Figure 5 that the bulge and the disk are very similar in colors redward of *V*. However, the disk exhibits a clear color gradient in the *V* and *B* colors of $d(I-V)/d\ln(r) = 0.32$ and $d(I-B)/d\ln(r) = 0.58$, respectively. Within the bulge the *B* and *V* gradients are similar to the disk's, but

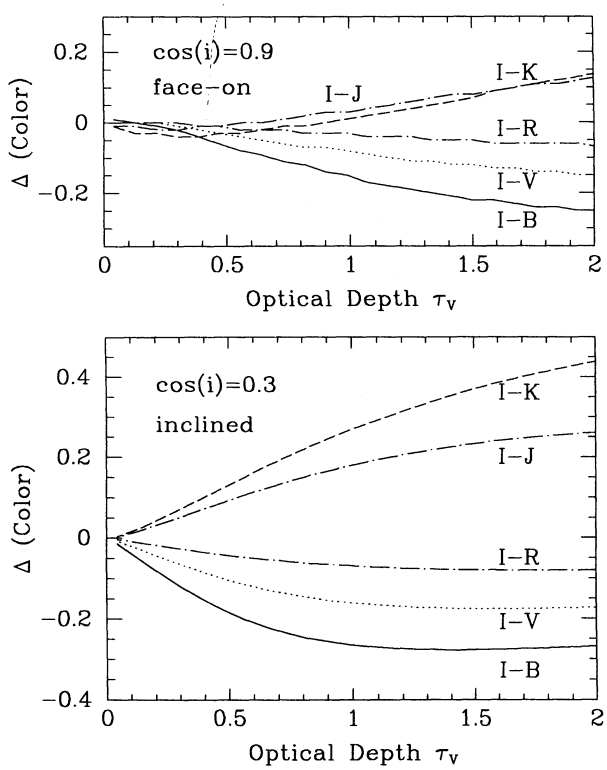

FIG. 6.—Model for color change in the presence of dust. This figure shows the expected color change, with respect to the unreddened case, for the star dust model described in the Appendix. The model assumes Gaussian stratifications of the dust and the stars, with a scale height ratio of ζ and a total optical depth of τ_V. Models with $\zeta = 0.4$ are shown for two inclinations: nearly face-on [cos (*i*) = 0.9] and highly inclined [cos (*i*) = 0.3]. It is noteworthy how little ($\lesssim$0.1 mag) the colors change for the face on case even as τ_V approaches unity. This is due to the high dust albedo in the optical which makes the dust layer reflective to radiation from in front of it.

there is a color offset toward the red of 0.3 mag in B and 0.15 mag in V.

The optical and IR color gradients of the bulge are worth being considered separately. Elliptical galaxies show relatively homogeneous properties in their optical to IR color gradients, $d(B-V)/d(V-K) = 0.25 \pm 0.08$ (Peletier 1989). The gradients in ellipticals are thought to arise principally as a result of a gradient in the metallicity. The attribution of these gradients to metallicity is also supported by the variation of $B-V$ with $V-K$, 0.33 ± 0.03, for a sample of field galaxies observed by Persson et al. (1979). This variation is between galaxies referenced to a fiducial fraction of the galaxy's light, and color variations between these galaxies result from the metallicity differences which are correlated with the luminosities and hence masses of the galaxies. We find a color gradient in the bulge of M51 of 0.51 ± 0.08, i.e., $V-K$ changes less than expected from the $B-V$ gradient.

We consider three possible causes for the size of M51's color gradient. First, it could arise from an extinction gradient with more dust covering the inner portion of the bulge than the outer portion. A simple screen with $A_V \approx 0.75$ at the center and declining to zero at 20″ would reproduce the $V-K$ gradient but could not simultaneously reproduce the gradients observed in the other colors. Inspection of Figure 6 indicates that more complicated dust models are not likely to produce the $d(B-V)/d(V-K)$ observed for M51's bulge. Second, M51's gradient could result from a change in the metallicity. Comparison with the gradients for ellipticals mentioned above suggests that this explanation may account for some portion of the gradient. The third possibility would account for the gradient through an outward decrease in the mean age of the stellar population. We examined the magnitude of the effect possible from an age change using models similar to those calculated in Rieke et al. (1993). A slope of $d(B-V)/d(V-K) = 0.39$ is derived for old galaxies with the $V-K$ gradient in M51's bulge corresponding to an age change of about 1 Gyr. Again, this explanation cannot alone account for the ratio of optical-to-infrared color gradient observed in M51's bulge.[5] We cannot separate age effects from metallicity effects with our limited set of colors, but the correct explanation for the gradients may well involve a combination of the two.

3.2. *The Structure of the Dust Lanes*

The apparent structure of M51 in the optical differs from its stellar surface mass distribution, at least in part, through the light obscuration in dust lanes and patches (Fig. 1). Before identifying variations in the K band image with surface mass variations we must assess the impact of those dust lanes at K. The structure of dust features in a sample of spiral galaxies has been studied carefully by Elmegreen (1980), based on optical photometry. She found that the optical depths in the lanes can be large, $\tau_V \approx 10$. The fact that the dust lanes and many dust patches appear so prominently in I band images (Fig. 1) implies that even at 8000 Å the optical depths in these regions are large. However, in the K band the dust lanes appear to be optically thin from Figures 1 and 2.

Aside from Elmegreen's (1980) study, there is very little information on the vertical geometry of the dust in galaxies outside the Milky Way. Kylafis & Bahcall (1987) and Wainscoat et al. (1990) made an estimate of the global scale height of the dust, relative to the stars, from the photometry of edge on galaxies. However, such estimates refer to the combined effects of smoothly distributed dust, diffuse dust, dust lanes, globules and warps in the disk. Since M51 is nearly face-on it allows local estimates of the vertical dust distribution.

Figure 7 shows the color changes of all other bands compared to K along two cuts perpendicularly across major dust lanes. These cuts show that the dust lanes are optically thin at K, semi-transparent at J and I, and optically thick at B, V, and R. We can make a reasonable estimate of the dust lanes' optical depths and z-heights with the simple model described in the Appendix. The models are parameterized by the optical depth at K, τ_K, and by the relative scale height of dust and stars, ζ. We assume that the optical depth outside the dust lane is negligible and that the unreddened colors do not change across the dust lane. The latter is supported by the similarity of the colors on either side of the dust lane, compared to the color changes across it (see Fig. 7).

The adopted color changes in $BVRIJ$ across the two lanes are listed in Table 2, along with estimates of their uncertainty. The quality of match between the radiative transfer models and the observations is given by

$$\chi^2(\tau_K, \zeta) = \sum_{\text{all colors } i} \frac{[\Delta C_i^{\text{pred}}(\tau_K, \zeta) - \Delta C_i^{\text{obs}}]^2}{\delta C_i^2} .$$

where ΔC_i is the color difference, $i - K$, between the center of the lane and the surrounding innerarm regions and δC_i is the error in this estimate. Contours of $\Delta\chi^2 \equiv \chi^2(\tau_K, \zeta) - \chi^2_{\min}(\tau_K, \zeta)$ are shown in Figure 8 for the range $0 < \zeta < 1$ and $0 < \tau_K < 1$.

The two examples show that optical depths in the dust lanes at K are about 0.5, corresponding to $\tau_V \sim 4$. These estimates are in agreement with Elmegreen's (1980) results. They also agree well with the optical depths expected from recent, high resolution CO column density measurements in the spiral arms of M51 (Rand & Kulkarni 1990), assuming a standard CO to dust conversion. At these optical depths the K band flux is attenuated only by $\sim 10\%$.

From analyzing several patches (e.g., Fig. 8), the relative scale height of the dust to the stars, ζ, is found to range from 0.25 to 0.6, decreasing with radius. Near the bulge, the dust's vertical distribution is comparable to the stars, while it is substantially flatter in the disk. However, in all cases the dust in the lanes appear to be more vertically extended than inferred from global edge-on estimates, $\langle\zeta\rangle = 0.2$.

TABLE 2

COLOR CHANGES ACROSS TWO PROMINENT DUST LANES WITH RESPECT TO K

Color ΔC	Lane 86 (mag)	Lane 45 (mag)
$J-K$	0.21 ± 0.04	0.13 ± 0.04
$I-K$	0.50 ± 0.04	0.38 ± 0.04
$R-K$	0.64 ± 0.04	0.53 ± 0.04
$V-K$	0.79 ± 0.04	0.58 ± 0.04
$B-K$	1.01 ± 0.04	0.69 ± 0.04

NOTE.—Color change refers the difference between the mean color on either side of the dust lane and the center.

[5] It must be noted that these statements exclude the "mini-AGN" region in the nucleus. The region with $r < 2''$ has colors substantially bluer than the surrounding bulge. Since for radii $r < 2''$ the different seeing conditions in the various bands make it hard to estimate colors, this region has been omitted from Fig. 5.

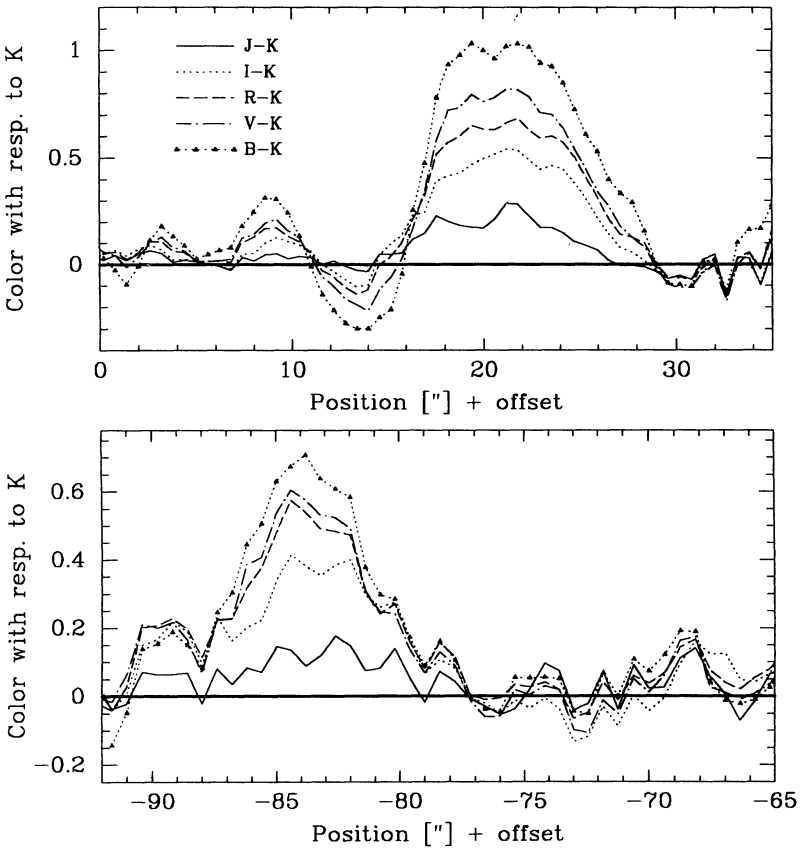

FIG. 7.—Color cut across dust lanes. This figure shows the color change across two dust lanes with respect to K in all other bands. The top panel shows a dust lane in the bulge/disk transition region ($\sim 25''$) and the bottom panel shows a lane in one of the dominant arms at $R \sim 90''$. As expected, the color changes become monotonically stronger toward bluer colors ($J-K$, $I-K$, $R-K$, $V-K$, and $B-K$).

3.3. *The Structure of the Spiral Arms*

One of the long-standing problems for testing models of spiral structure in detail has been the difficulty in mapping surface mass variations quantitatively. These variations should be reflected in smooth surface brightness variations of the old stellar population. However, in optical images of spirals, the most conspicuous variations are caused by dust lanes and by young stars. Even though Schweizer's (1976) work has shown that there is a smooth underlying variation in the red light, its quantitative assessment has proven difficult, because even images at I are afflicted by dust extinction and by population changes across the spiral arms. The uncertainties about the basic structural parameters are best illustrated by the conflicting claims found in the literature:

1. Schweizer (1976) estimates an arm/interarm contrast of $\pm 20\%$ at the radii of the outermost H II regions ($\approx 250''$), while Elmegreen et al. (1989) estimate the contrast to be more than two magnitudes at the same radii.

2. Elmegreen, Elmegreen, & Seiden (1989) claim that the B and I spiral arm amplitudes are comparable, indicating a density wave rather than a population change, while Wright, Casali, & Walther (1991) claim that the K band amplitude is a factor of 2 lower than at I, implying that not even the I band light traces the old disk population.

3.3.1. *Localized Optical-IR Comparison of the Spiral Arms*

As a starting point we compare the I band and K band properties of the spiral arms, because the I band has been conventionally used (Schweizer 1976; Elmegreen et al. 1989; Kaufman et al. 1989) to assess the dynamical structure of spiral galaxies.

A visual comparison of the I and K band images in Figure 1 shows that many discrete clumps and point sources (mostly OB associations) are nearly as prominent in K as they are at I; indeed a few appear only at K because they are completely obliterated by dust at I. However, these clumps occupy only a very small fraction of the spiral arms. The most dramatic difference between I and K is in the appearance of the dust lanes: while at I the dust lanes are still prominent (reducing the observed peak flux to nearly half in some places), they are discernible at K only just outside the bar (at $r \approx 15''$).

The differences are highlighted in the $J-K$ color map, shown in Figure 2*d*. A more quantitative impression of these color differences, $\Delta(I-K)$ of up to 0.5, is given in two cuts perpendicularly across the spiral arm shown in Figure 7. Thus the local structure of the spiral arm (e.g., the location and the amplitude of the density maximum) is inadequately described by the I band data (see also Fig. 12 below).

3.3.2. *How Much Do Young, Red Stars Contaminate The K Band Image?*

Aside from dust obscuration, the spiral amplitude of the light may differ from the mass through contamination by young stars. In addition to the blue hot young stars, cool, red supergiants (RSGs) appear in a young stellar population after 5 million years. These stars emit most of their light in the near

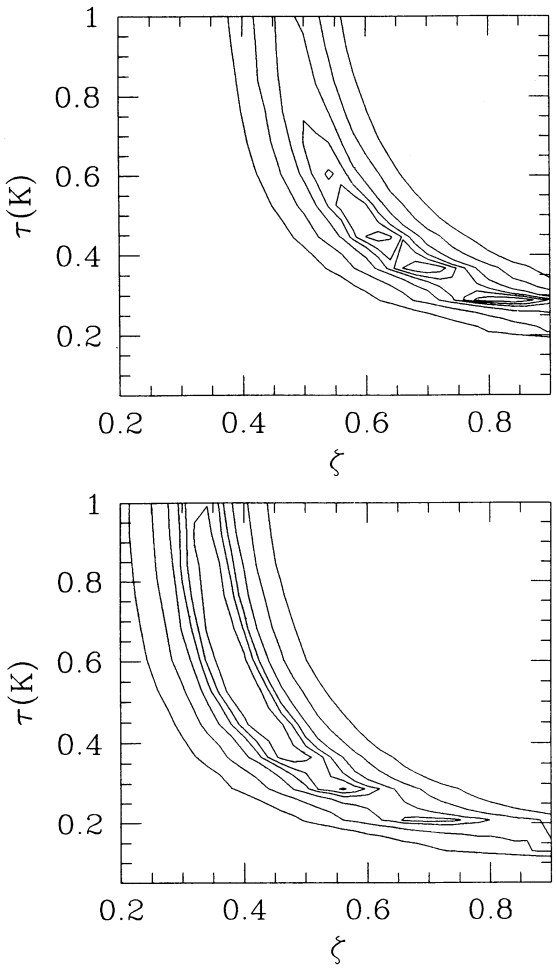

FIG. 8.—Confidence limits in the $\tau_V - \zeta$ plane for two dust lanes. This figure shows confindence limits in the $\tau_K - \zeta$ plane when applying the models from the Appendix to the color changes shown in Fig. 7. The contours are spaced by $\Delta\chi^2 = 3$ compared to the best model. For the dust lane at 25″ the optical depth at K is found to be ~0.4 (corresponding to $\tau_V \sim 3.5$) with a scale height of 60% of the star's. For the dust lane in the disk (*lower panel*) the dust scale height is only ~35% of the star's, and the optical depth is constrained to be $\tau_K = 0.4$–1, corresponding to $\tau_V = 3.5$–9.

infrared, and could contribute a significant fraction of the K light in the spiral arms and hence could spoil the K band light as a tracer of the surface density variation. The relevant definition of "young" here implies that the stars were born near the crest of the spiral wave and have not yet had time to drift away from spiral arm. The radial distance by which a star will have moved from its birth position, relative to the spiral density pattern, can be estimated as

$$\Delta R \sim \Omega_p R T \sin(i) ,$$

where R is the distance from the galaxy center, Ω_p is the pattern speed at R, T is the age of the star, and sin (i) is the pitch angle of the spiral arm.

In a single age population (e.g., formed by the density wave shock), RSGs contribute most to the K light after about 1.5×10^7 yr (e.g., Rieke et al. 1993). At an $R = 25''$, or about 1 kpc, in M51 this translates into a maximum supergiant contribution at $\Delta R = 9''$ outside the dust lane (their approximate birth place), where we have assumed $\Omega_p \approx 60$ km s^{-1} kpc^{-1} and sin (i) = 15° (Tully 1974). Thus if, RSGs contribute to the K band spiral amplitude they are expected to do so significantly further away from the dust lane than the OB associations. Since these stars also had more time to disperse they will not appear as tightly clumped as the OB associations.

An inter-arm comparison of the strength of CO molecular absorption at CO(2.3 μm), which is strongest in cool supergiants with low surface gravities, enables us to estimate observationally the contribution of RSGs to the K light near the spiral arms (Fig. 9). This test for population changes has the great advantage that it compares fluxes at nearly identical effective wavelengths and is therefore independent of dust extinction. For a single aged population K − CO can differ by 0.1–0.15 mag compared to an aged ($T \gg 10^8$ yr) population of the same metallicity (Rieke et al. 1993). Figure 9 shows the K and CO profiles across the inner spiral arms at two positions, spanning the extremes found in the data set. In the one arm near the bulge K − CO does not change measurably across the arm, $\Delta(K - \mathrm{CO}) \lesssim 0.025$ mag, thus at most 20% of the light could arise from supergiants. In the second arm $\Delta(K - \mathrm{CO}) \sim 0.1$ over a small localized region, indicating that much of the light in this patch comes from RSG. The region of strong CO is about 6″ outside the density crest of the spiral arm, consistent with the hypothesis that these RSGs were born just inside the crest 15 million years ago. However, significant changes of K − CO were found only in one single, localized region. Thus at most small portions of the spiral arm at K have large contributions from young star light while the rest traces mostly an old population.

3.3.3. *Harmonic Decomposition of the Spiral Pattern and Global Amplitudes*

The most straightforward way of presenting quantitative information about the spiral arms is to decompose the disk light into its harmonic, or Fourier, components in concentric annuli, after having corrected for the inclination of the galaxy

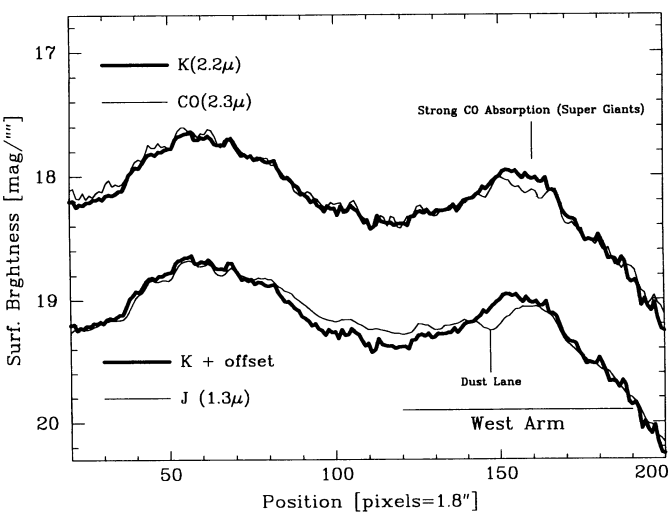

FIG. 9.—K − CO(2.3 μm) change across spiral arms. This figures compares the K band to the CO(2.3 μm) narrow band profiles along a cut that crosses (E-W) two spirals arms. Since the depth of the CO(2.3 μm) is a strong function of surface gravity, a dip in the CO(2.3 μm) profile, compared to K, is expected if much of the K light comes from young, red supergiants. This cut shows the only place in the inner 2.'5 × 2.'5 where supergiants appear to be important contributors to the K band light, just outside the crest of the spiral arm (around pixels 160). Below we compare the K and J light profiles along the same cut. This comparison shows a smooth color change between arm and interarm region of (~0.1 mag) and the main dust lane (near pixel 150).

(e.g., Grosbol 1987; Elmegreen et al. 1989, Elmegreen, Elmegreen, & Montenegro 1992). It would also be possible to decompose M51 into a set of logarithmic spirals (e.g., Considere & Athanassoula 1988), but we have not pursued this decomposition because the spiral arms in M51 are not well approximated by logarithmic spirals.

Following Tully (1974) we assumed an inclination of $\sim 25° \pm 5°$, to transform the images to face-on.[6] For radii between 20″ and 210″ we formed 30 azimuthal bins by medianizing the pixel values within segments of 12° in angular extent and of $R_{max}/R_{min} = 1.05$ in radial extent. Taking the median over the sampling area reduces the impact of point sources. Alternatively, we gave zero weight to pixels with strong point sources and averaged over the rest. Both methods yielded very similar results.

The power in the harmonic components from $m = 1$ to $m = 6$ is shown in Figure 10 for the K band image as a function of radius. The power in $m = 1$ signifies the lopsidedness of the disk, presumably due to the interaction with NGC 5195. Aside from $m = 1$ most of the power is in the $m = 2$ component, reflecting the strong two arm spiral. The local maximum at $R = 15''$ is the imprint of the central bar onto the $m = 2$ component. Significant, but much less, power is also found in the $m = 4$ and $m = 6$ components, because the two spiral arms are more localized than a simple double sinusoidal wave, i.e., the inner arm regions are wider than the arms. There is only little power in the higher order components with odd symmetry. There is also very little power in even components higher than $m = 6$; hence a Fourier decomposition up to $m = 6$ yields a good representation of the galaxy image.

Even though we have argued above on the basis of the $K - CO(2.3\ \mu m)$ comparison that the K band amplitude is not significantly affected by population changes, it is useful to employ the multicolor information to check this. Figure 11 compares the radial dependence of the $m = 2$ component at K and at V. The qualitative, global amplitude structure is common to both wavebands, showing two pronounced minima at 45″ and 170″ and a maximum at 120″. At 70″ and 120″, the optical colors exhibit an amplitude which is 30% lower than at K. These are the radii at which the dust lanes, which are optically thick at all wavelengths except K, are most extensive. This difference suggests that at least one-third of the flux in the spiral crest is absorbed by dust in the optical bands, consistent with the optical depth estimates from § 3.3.

To obtain some estimate for the peak-to-valley amplitude of the two arm spiral density contrast we must use more information than the $m = 2$ amplitude, because the spiral arms are more peaked than a doubly sinusoidal curve. In Figure 12 we show the sum of all *even* components up to $m = 8$ at four radii. The K band amplitude rises from $I_{max}/I_{min} \approx 1.8$ at $R = 70''$ to a factor of 3 at $R = 125''$ and falling back to a factor of 2 at $R = 150''$. These values for the amplitude of the mass tracing stellar population are a factor of 3 to 5 higher than estimated by Schweizer (1976) for M51, but are a factor of 1.5 to 2 lower than estimated by Elmegreen et al. (1989). Furthermore, as is already evident from the $m = 2$ component, the amplitudes at I and K are comparable with K being somewhat higher; this finding is in contrast with Wright et al.'s (1991) claim that the K band amplitude is a factor of 2 lower than the I band amplitude.

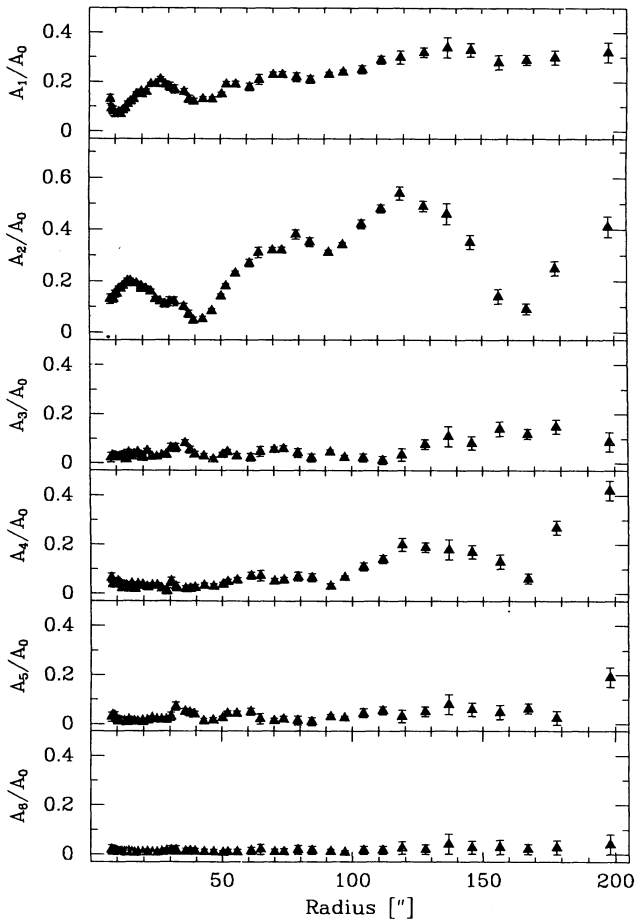

FIG. 10.—Harmonic decomposition of the spiral arms at K. This figure shows the result of a Fourier decomposition in azimuth of the intensity in concentric annuli of the K band image. The K band image had been corrected to face-on. The panels show the $m = 1 \ldots 6$ Fourier amplitudes, normalized by the mean flux in each annulus. There is a nonzero $m = 1$ component at all radii, indicating the lopsidedness of M51. The dominant component is $m = 2$, arising in the inner parts $R \lesssim 25''$ from the central bar and in the outer parts from the strong two arm spiral. Note the clear minima in the radial run of the $m = 2$ amplitude at 45″ and 170″. There is significant power in the $m = 4$ component, because the two arm spiral is a more compact feature than a doubly sinusoidal wave. The power in all odd components, except $m = 1$ is small ($\lesssim 10\%$).

Such a large arm/inter-arm contrast ($\Delta\Sigma/\langle\Sigma\rangle > 1$) seems to be in accord with N-body simulations of tidal encounters similar to that one that M51 seems to have just undergone. Toomre & Toomre (1972) Hernquist (1990), and Sundelius (1990) have shown that spiral features resulting from tidal encounters can have density contrasts in excess of unity. However, so far no detailed analysis of the radial dependence of the arm amplitude, as in our Figures 10 and 11, has been published for these simulations. The data presented here should permit a straightforward comparison.

Elmegreen et al. (1992) recently have presented evidence that many spiral galaxies have significant $m = 3$ arms, even though they may not be apparent in visual inspection. In M51 they find evidence for three arm spirals between the radii of 50″ and 100″. In Figure 11 we present multicolor information on the radial run of the power in the $m = 3$ component. It becomes

[6] For nearly face-on galaxies the projected velocities vary strongly with the assumed inclination, while the projected surface brightness does not. Therefore, this deprojection based on a kinematic inclination estimate is insensitive to the exact inclination assumed.

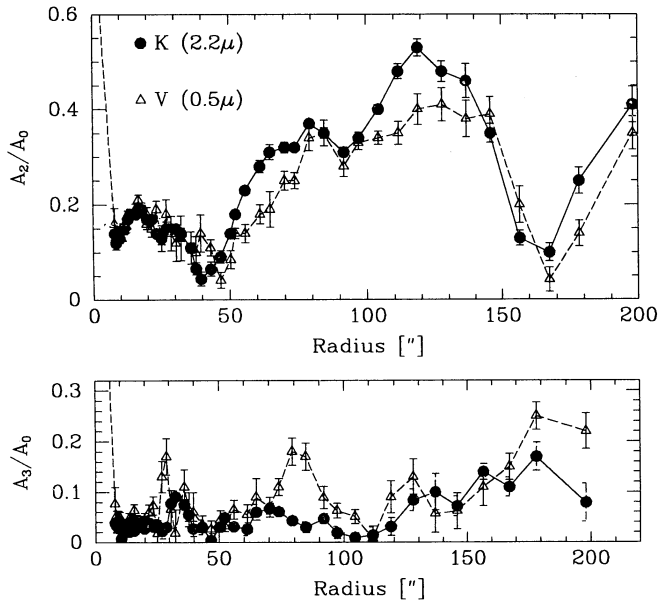

FIG. 11.—$K-V$ comparison of the harmonic decomposition. This figure compres the $m = 2$ and the $m = 3$ azimuthal components in V and K. For the $m = 2$ component the V and K amplitudes trace each other at least qualitatively. Note that at some radii the K band image has about 25% more $m = 2$ power, because the signal is suppressed by dust in the optical. Thus the two arm spirals are more prominent in K than in the optical. Even though the V band seems to show significant $m = 3$ power at $\sim 70''$, such a feature is not present in K. Thus there is no massive three-armed spiral in M51.

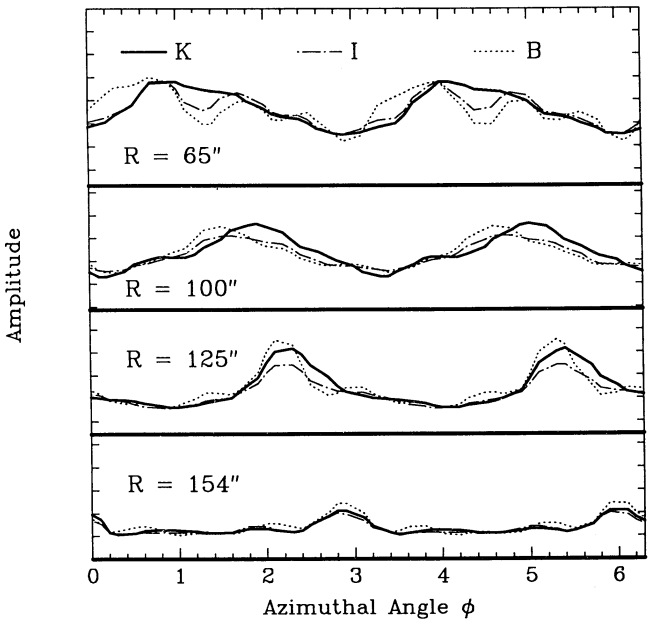

FIG. 12.—Arm-interarm density contrast. This figure shows the symmetrized azimuthal brightness variations (in B, I, and K) at four different radii, obtained by adding all even Fourier components up to $m = 8$. The solid line represents the K band variation and is expected to be a good approximation (see § 4.3.2) to the surface mass density variations. The I band profiles (*dashed lines*) already show the significant impact of the dust lane (to the right of the crest). The B band profile (*dotted line*) shows both the impact of dust as well as the young blue stars on the trailing (*left side*) side of the crest. This figure shows that the arm-interarm contrast in K is as large as 3.

apparent from this figure that the power in this component is strongly color-dependent, decreasing in amplitude toward redder passbands. We are hence led to conclude that these features in M51 are not dynamical features, tracing mass, but rather features in gas and dust only.

4. CONCLUSIONS

The main conclusions of this paper are as follows:

1. Quantitative IR surface photometry (J, K, CO) is possible down to surface brightnesses of $\mu_K \sim 20$ mag, with an accuracy of 0.06 mag. Differential measurements are accurate to 0.03 mag. Thus even for face-on spiral galaxies IR-array detectors can provide high-quality surface photometry over several disk scale lengths, in the present case to a radius $R \sim 0.7R_{25}$.

2. Even though the optical colors of face-on disks are surprisingly insensitive to a smooth distribution of dust, we can place limits on the global optical depth of M51's disk of $\langle \tau_V \rangle \lesssim 1$–2, if the dust has a radial scale length comparable to the stars'. The dust in M51 removes a significant fraction of emission from the spiral arm crest at all wavelengths less than 1 μm; this causes the spiral arm amplitude at K(2.2 μm) to exceed the one at I(0.8 μm). The major dust lanes have an optical depth of $\tau_K \sim 0.4$, indicating an amount of dust in the arms compatible with the amount of molecular gas found there. The relative scale heights of dust and stars, ζ, is found to be $\sim$0.2–0.6. Because M51 is seen face-on, the fraction of radiation at K(2.2 μm) removed by the dust does not exceed $\sim$10%, even in the main dust lanes.

3. We were able to show from measuring the CO(2.3 μm) molecular band strength across spiral arms that in localized regions young, red supergiants contribute significantly to the K band flux. Since these regions are found to be small, this provides the first well founded evidence that even in star-forming galaxies K band images *are indeed good tracers of the massive, older disk population.* Hence, in face-on galaxies variations in the K band can be straightforwardly interpreted as variations in the stellar disk mass density. Only on scales as small as dust lanes there remains a significant ($\sim$10%) uncertainty in this mapping.

4. The spiral arm amplitude in M51, as reflected in the K band image, is large: a factor $\gtrsim 3$ at some radii. This finding is intermediate to previous claims which were discrepant by an order of magnitude. Such a large amplitude appears to be in accord with N-body simulations of tidal encounters similar to M51/N5495. The spiral arm amplitude exhibits well defined radial variations with two pronounced minima at 45" and 170".

5. We find that although the two arm spiral is clearly a mass feature, the reported features with threefold symmetry are color-dependent, nearly disappearing at K. Hence, these features with $m = 3$ are most likely to be present only in the dust and the gas, but not in the stars.

This and other imaging studies of spiral galaxies with infrared array detectors show that spiral galaxies look quite different in the IR (2.2 μm) than at I(0.8 μm), the longest wavelength at which they had been studied in detail so far. In particular small bars are common and the spiral arms seem to be strong. With imaging at K there finally is a direct way to map the stellar mass distribution in spiral galaxies in detail, relatively unafflicted by dust and young stars. Clearly, M51 with its peculiar interaction history does not allow generalizations to the properties of isolated spiral galaxies, but only enables a direct comparison with numerical simulations (e.g., Hernquist 1990). Nevertheless, it is a good test case to establish the usefulness of IR surface photometry to map the dynamical structure of the galaxy. Ongoing studies of samples of spiral galaxies will allow

a more complete survey for bars, will allow a check on how the spiral arm amplitude correlates with the current star-formation rate and will show how density wave resonances are reflected in the radial variations of the spiral arm amplitude.

H. W. R. was supported by a Hubble fellowship grant (HF-1024.01-91A) and financial support for the NICMOS2 and NICMOS3 cameras was provided by the National Science Foundation.

APPENDIX

In this Appendix we briefly describe the radiative transfer calculation used to estimate the expected color changes due to dust. The treatment here is very similar to the one described by Elmegreen (1980). We assume that both the stars and the dust are stratified in plane-parallel geometry. The vertical density profile is assumed to be a Gaussian for both components, with scale heights $\beta_{\rm star}$ and $\beta_{\rm dust}$:

$$\kappa(z) = \kappa_0 \exp\left(-\frac{z^2}{2\beta_{\rm dust}^2}\right),$$

$$j(z) = j_0 \exp\left(-\frac{z^2}{2\beta_{\rm stars}^2}\right),$$

where j is the volume emissivity of the stars and κ is the total cross section per unit length of the dust. Both j and κ are of course functions of wavelength. To calculate colors with respect to the unreddened case, it is sufficient to specify each model by $\zeta \equiv \beta_{\rm dust}/\beta_{\rm stars}$ and by the total optical depth at fiducial wavelength

$$\tau \equiv \int_{-\infty}^{\infty} \kappa(z)dz = \sqrt{2\pi}\kappa_0 \beta_{\rm dust}\,.$$

We only include absorption and isotropic scattering into the dust cross section, $\kappa = \kappa_{\rm abs} + \sigma_{\rm iso}$, with values for various wavelengths given by Draine & Lee (1984). The (isotropic) albedo is denoted as $\omega \equiv \sigma_{\rm iso}/\kappa$. As a further simplification we treat single scattering only and neglect multiple scattering. This implies that

$$I(\mu, z') = \frac{1}{\mu}\int_{-\infty}^{z'} j(z'') \exp\left(\frac{\tau'' - \tau'}{\mu}\right)dz''$$

for $\mu > 0$ [where $\mu = \cos(\theta)$ and θ is the angle with respect to the normal vector of the stratification]. For $\mu < 0$, $I(\mu, z') = -I(-\mu, -z)$.

The mean intensity $J(z)$ at a height z is defined as

$$J(z') = 2\pi \int_{-1}^{1} I(\mu', z')d\mu'$$

We can now calculate for each wavelength and each optical depth the intensity emerging from the surface at an angle μ as

$$I_\infty(\mu) = \frac{1}{\mu}\left\{\int_{-\infty}^{\infty}\left[j(z') + \frac{\omega}{2}\kappa(z')J(z')\right]\exp\left(\frac{\tau' - \tau}{\mu}\right)dz'\right\}.$$

This allows us to calculate the color change (§ 4.1) in the observed bands (with respect to the unobscured case) for a disk seen at inclination μ for various optical depths, specified by, say, τ_V. Alternatively, we can for each wavelength calculate the expected flux attenuation across a dust lane (§ 4.2) with optical depth, τ (assuming that the optical depth outside the lane is much smaller).

REFERENCES

Aaronson, M. 1977, Ph.D. thesis, Harvard Univ.
Boroson, T., Strom, K., & Strom, S. 1983, ApJ, 274, 39
Bothun, G., Mould, J., Schommer, B., & Aaronson, M. 1985, ApJ, 291, 586
Bruzual, G. A., Magris, G. C., & Calvet, N. 1988, ApJ, 333, 673
Considere, S., & Athanassoula, E. 1988, A&AS, 76, 365
de Vaucouleurs, G., de Vaucouleurs, A., & Corwin, H. 1976, Second Reference Catalog of Galaxies (Austin: Univ. Texas Press)
Disney, M., Davies, J., & Phillips, S. 1989, MNRAS, 239, 939
Draine, B. T., & Lee, H. M. 1984, ApJ, 285, 89
Elmegreen, B., Elmegreen, D., & Montenegro, L. 1992, ApJS, 79, 37
Elmegreen, D. 1980, ApJS, 43, 37
Elmegreen, B., Elmegreen, D., & Seiden, P. 1989, ApJ, 343, 602
Frogel, J., Persson, S., Aaronson, M., & Matthews, K. 1978, ApJ, 220, 75
Grosbøl, P. 1987, in "Selected Topics on Data Analysis in Astronomy," ed. L. Scarsi, V. DiGesu, & P. Crane (Singapore: World Scientific), 57
Hernquist, L. 1990, in Dynamics and Interactions of Galaxies, ed. R. Wielen (Berlin: Springer), 108
Kaufman, M., Bash, F., Hine, B., Rots, A., Elmegreen, D., & Hodge, W. 1989, ApJ, 345, 674
Kylafis, N., & Bahcall, J. N. 1987, ApJ, 317, 637
Peletier, R. 1989, Ph.D. thesis, Univ. Groningen
Peletier, R., & Willner, S. 1991, ApJ, 382, 382
———. 1992, AJ, 103, 1761
Persson, S., Frogel, J., & Aaronson, M. 1979, ApJS, 39, 61
Rand, R., & Kulkarni, S. 1990, ApJ, 349, L43
Rieke, G., Loken, K., Rieke, M., & Tamblyn, P. 1993, ApJ, 412, 99
Rix, H.-W. 1991, Ph.D. thesis, Univ. Arizona
Schild, R. 1983, AJ, 95, 1021
Schweizer, F. 1976, ApJS, 31, 313
Sundelius, B. 1990, in Dynamics and Interactions of Galaxies, ed. R. Wielen (Berlin: Springer), 118
Toomre, A., & Toomre, J. 1972, ApJ, 178, 623
Tully, R. 1974, ApJS, 27, 449
Valentijn, E. A. 1990, Nature, 346, 153
Wainscoat, R., Hyland, A., & Freeman, K. 1990, ApJ, 348, 85
Witt, A. N., Thronson, H. A., & Capuano, J. M. 1992, ApJ, 393, 611
Wright, G., Casali, M., & Walther, D. 1991, in Astrophysics with IR Arrays, ed. R. Elston (Cambridge: Cambridge Univ. Press), 44
Zaritsky, D., Rix, H.-W., & Rieke, M. 1993, Nature, in press